ACS OMEGA

Article

Cite This: ACS Omega 2019, 4, 11728−11736

http://pubs.acs.org/journal/acsodf

pH-Labile Magnetic Nanocarriers for Intracellular Drug Delivery to Tumor Cells

Santosh L. Gawali,[†,‡] Kanhu C. Barick,*[,†,‡] Neena G. Shetake,[‡,§] Vasumathy Rajan,[§] Badri. N. Pandey,[‡,§] N. Naveen Kumar,[∥] K. Indira Priyadarsini,[†,‡] and Puthussericka A. Hassan*[,†,‡]

[†]Chemistry Division, [§]Radiation Biology and Health Sciences Division, and [∥]Materials Science Division, Bhabha Atomic Research Centre, Trombay, Mumbai 400085, India

[‡]Homi Bhabha National Institute, Anushaktinagar, Mumbai 400094, India

Supporting Information

ABSTRACT: We report the development of pH-labile ascorbic acid-coated magnetic nanocarriers (AMNCs) for effective delivery of the anticancer drug doxorubicin hydrochloride (DOX) to tumor cells. The uniqueness of this drug delivery system lies in the covalent conjugation of DOX through carbamate and hydrazone bonds, resulting in a slow and sustained drug release profile at different environmental acidities. X-ray diffraction and transmission electron microscopy analyses reveal the formation of crystalline single-phase Fe_3O_4 nanoparticles with an average size of 10 nm. The changes in the interfacial characteristics of the nanocarriers and the presence of organic coatings are probed by infrared spectroscopy, dynamic light scattering, zeta potential, and thermogravimetric measurements. AMNCs show high colloidal stability in aqueous and cell culture media and possess good magnetic field responsivity and protein resistance characteristics. The drug-loaded nanocarriers exhibited sustained pH-triggered release of drug molecules in acidic mediums, substantial cellular internalization, and significant toxicity toward the proliferation of mouse skin fibrosarcoma (WEHI-164), human breast cancer (MCF-7), and human lung cancer (A549) cells. However, it showed significantly lower toxicity in human normal lung (WI26VA) cells. Overall, these results suggest a pH-sensitive drug release of nanoformulations, which showed selective toxicity to tumor than normal cells.

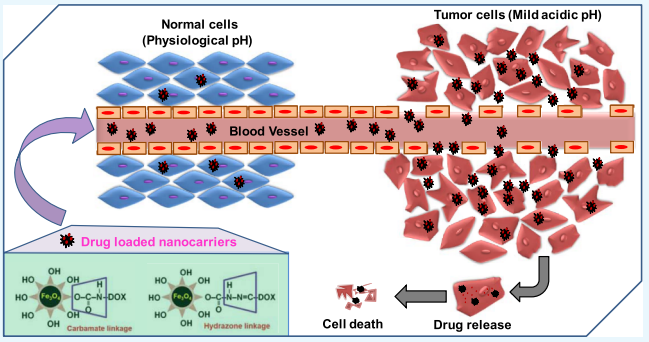

1. INTRODUCTION

Conventional chemotherapies for cancer suffer from the disadvantage of toxicity to normal cells and nonspecific biodistribution, leading to toxicities to organs like livers, kidneys, and so forth.[1] Targeting of the drug to the tumors can be achieved by incorporating the active ingredient in suitable nanostructured materials with desired size, charge, and surface characteristics.[2] Magnetic nanoparticles (MNPs) conjugated with drugs have been assessed as a strategy to deliver anticancer agents to tumor sites.[3] In addition to the targeting capability, most of these nanocarriers solve other limitations of conventional drug delivery systems in terms of solubility, systemic toxicity, and drug degradation. The rationale behind this approach is to increase efficacy, while reducing systemic side-effects.

Among others, superparamagnetic Fe_3O_4 nanoparticles are widely favored because of biocompatibility, unique physiochemical properties, and reactive surfaces that can be readily modified by functionalizing with suitable surface-passivating agents.[4−7] Another advantage of using Fe_3O_4 MNPs as nanocarriers is that they are biodegradable through the iron metabolism pathway. An important step in developing such nanocarriers is to modify the surface of Fe_3O_4 MNPs with suitable organic/inorganic species that have targeting sites, pH-sensitive moieties, and ability to conjugate drugs/biomarkers.[7−12] Ascorbic acid (AA) is one of the most essential vitamins for both pharmaceutical and food-processing industries. It contains four −OH groups (two enol −OH groups on lactone ring carbons and two −OH groups on the side chain C atoms) and a carbonyl group (lactone ring carbons). AA as well as its oxidized product dehydroascorbic acid (DHA) act as good capping agents because of the chemical interaction of its carbonyl group with metal ions.[13−15] AA is highly water-soluble and it shows strong antioxidant properties[16,17] and hence, significant interest lies in preparing highly water-dispersible Fe_3O_4 MNPs using AA as a capping agent for biomedical applications. Sreeja et al. and Gupta et al. reported the magnetic resonance contrast properties of AA- and DHA-coated MNPs, respectively.[13,14] However, the drug delivery capability of AA-conjugated nanoparticles is not explored. AA is transported into cells in DHA form via the glucose transporter (GLUT) protein.[18] Enhanced GLUT

Received: April 15, 2019
Accepted: May 22, 2019
Published: July 5, 2019

DOI: 10.1021/acsomega.9b01062
ACS Omega 2019, 4, 11728−11736

Scheme 1. Schematic Representation of Covalent Linkage of DOX to AMNCs

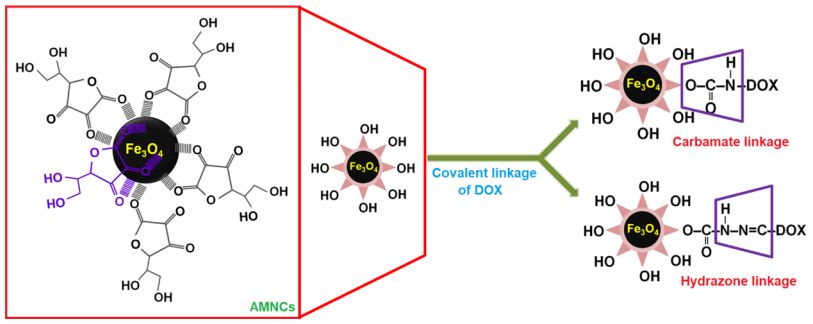

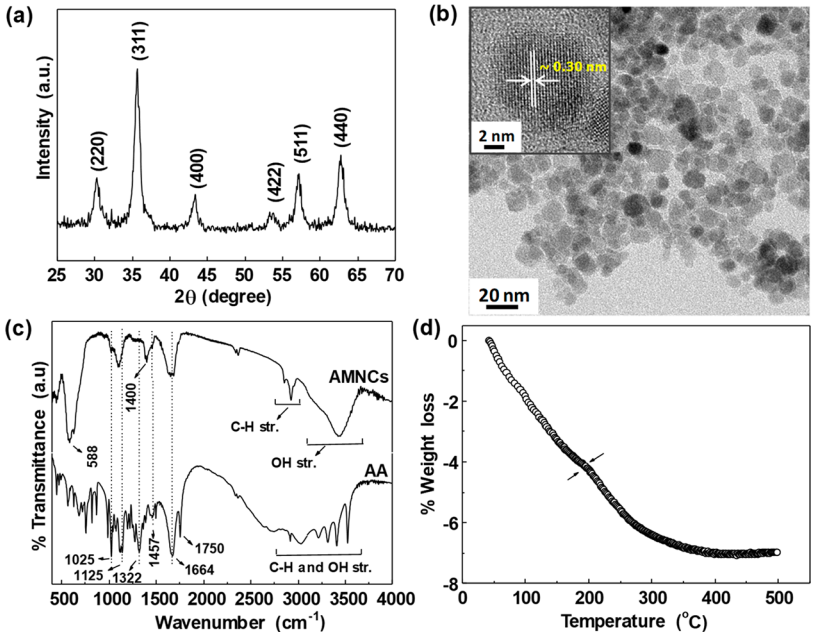

Figure 1. (a) XRD pattern and (b) TEM image (inset: HRTEM image), (c) FTIR spectra (along with pure AA) and (d) thermogravimetric analysis (TGA) plot of AMNCs.

expression has been reported in various cancers such as hepatic, breast, pancreatic, brain, renal, esophageal, lung, colorectal, endometrial, cutaneous, cervical and ovarian carcinoma, and so forth.[19] Therefore, higher intracellular delivery of anticancer drugs can be achieved by using AA-conjugated nanoparticles as drug carriers. Further, DHA can cross the blood brain barrier by GLUT1[20] and thus, AA-conjugated nanoparticles can also be useful for brain drug delivery. Although many noncovalent approaches have been employed for delivering anticancer drugs, the in vivo stability of the drug delivery system constructed using a noncovalent method is still challenging. The drug delivery systems formed by covalent approaches (via chemical bonds) provide more stability to drugs as well as their selective release than those constructed using noncovalent linkages.[21−25] In this aspect, polymer−drug conjugates are extensively developed by using pH-labile chemical bonds such as hydrazone, cisacotinyl, carbamate, and acetal bonds.[26−28] The presence of acid-labile linkages between drugs and polymeric carriers permits drug release either in the mild acidic extracellular environment of a tumor or after endocytosis in endosomes or lysosomes in tumor cells.

Herein, we report development of pH-labile magnetic nanocarriers for effective delivery of anticancer drug, DOX, to tumor cells. DOX was covalently bound to the ascorbic acid-coated magnetic nanocarriers (AMNCs) through carbamate and hydrazone linkage (Scheme 1). The developed drug−nanocarrier conjugate would minimize the amounts of drug leaching out in the blood (pH 7.4) and enable drug release upon being internalized by the target cells (pH 5). It is noteworthy to mention that these colloidally stable, pH-sensitive nanocarriers showed selective toxicity to tumor than normal cells.

2. RESULTS AND DISCUSSION

2.1. Structural and Magnetic Property Studies. An X-ray diffraction (XRD) pattern (Figure 1a) confirmed the formation of a single-phase inverse cubic spinel Fe_3O_4 nanostructure. The lattice constant was found to be 8.378 Å, which is very close to the reported value of Fe_3O_4 (JCPDS card no. 88-0315, a = 8.375 Å). From X-ray line broadening, the crystallite sizes were estimated to be ∼9.7 nm. A transmission electron microscopy (TEM) micrograph (Figure 1b) also shows the formation of almost spherical-shaped Fe_3O_4 nanoparticles of an average size of ∼9.5 nm (particle size distribution is shown in Figure S1a, Supporting Information). High-resolution TEM (HRTEM) analysis confirmed that each particle is highly crystalline and single-domain. The average

DOI: 10.1021/acsomega.9b01062
ACS Omega 2019, 4, 11728−11736

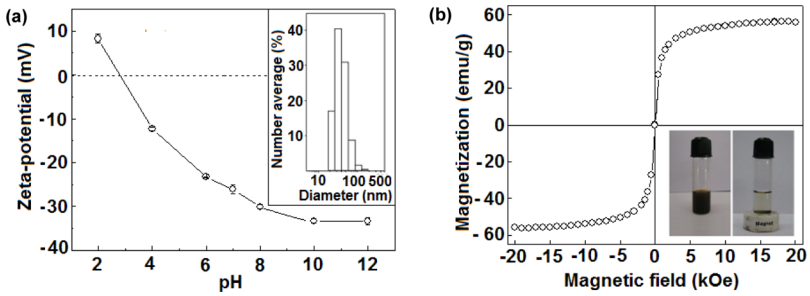

Figure 2. (a) pH-dependent zeta potential plot (inset shows its DLS plot indicating the hydrodynamic diameter of the particles) and (b) room temperature field dependence of magnetization (M vs H) plot of AMNCs (inset shows the photographs of its aqueous suspension in the presence and absence of a magnetic field).

interplanar distance (inset of Figure 1b) was measured to be ~0.30 nm, which corresponds to the (220) lattice plane of Fe_3O_4.[7] Further, the selected area electron diffraction pattern (Figure S1b, Supporting Information) also confirmed the high crystalline nature of AMNCs.

The successful conjugation of AA on the surface of Fe_3O_4 MNPs is confirmed by Fourier transform infrared (FTIR) and thermal analyses. From the FTIR spectra (Figure 1c), it is seen that vibrational bands for pure AA are prominently resolved, but those of AMNCs are relatively broad and few. The intense peak that appeared at around 588 cm^{-1} in the spectra of AMNCs can be attributed to the Fe−O vibration of Fe_3O_4 MNPs.[7] AA exhibited bands at 1750, 1664, and 1322 cm^{-1} for C═O stretching of a five-member lactone ring, C═C stretching vibrations coupled with the neighboring vibrations along the conjugated system, and enol hydroxyl stretching vibrations, respectively.[15] The C═C and enol hydroxyl stretching vibrations of AA also appeared in the FTIR spectrum of AMNCs. The absence of an intense C═O stretching band in AMNCs indicates that the oxygen atom of the carbonyl group has coordinated with the Fe atoms of the MNPs surface (through C═O···Fe interaction). This coordination is further confirmed by the appearance of a new intense vibrational band at 1400 cm^{-1}. However, it is difficult to predict whether Fe is coordinated with AA using one, two, or three of its C═O groups of the lactone ring. The band appearing at 1125 and 1025 cm^{-1} in pure AA can be associated with C−O groups of the lactone ring.[14] These peaks appeared in the spectrum of AMNCs with a slight shift in peak position. Further, the bands corresponding to different hydroxyl groups of AA in the range of 3210−3527 cm^{-1} appeared as a broad band in the FTIR spectrum of AMNCs. TGA (Figure 1d) showed a two-step decomposition of AMNCs with a total weight loss of about 7%. The first step of weight loss up to 200 °C can be ascribed to the removal of physically absorbed water and AA molecules, whereas weight loss beyond this can be associated with removal of chemically adsorbed AA and any chemisorbed water molecules, if present, from the surface of Fe_3O_4 nanoparticles. Previous studies indicate that bare Fe_3O_4 nanoparticles prepared by a similar method without using any coating agent exhibit about 2.5% weight loss owing to the removal of both physically and chemically adsorbed water molecules.[29] As the total weight loss beyond 200 °C is much more than 2.5%, it is inferred that there is a significant contribution from the decomposition of chemisorbed AA. This supports efficient capping of Fe_3O_4 nanoparticles by AA molecules. It has been reported that pure AA starts decomposing at about 191 °C and experiences the maximum rate of decomposition at about 221 °C.[30] This shifting of decomposition temperature to higher degrees for AMNCs can be attributed to the chemical coordination of AA with Fe_3O_4 nanoparticles. The weight loss observed by TGA was further supported by iron estimation (through the phenanthroline spectrophotometric method),[31] which showed that about 8% organic moieties are present on the particle. Thus, FTIR and TGA provide a clear evidence of effective capping of AA on the surface of Fe_3O_4 nanoparticles.

Light scattering measurements were performed to determine the hydrodynamic diameter and surface charge of these particles in aqueous medium. From pH-dependent zeta potential measurements (Figure 2a), the point of zero charge (PZC) of AMNCs was found to be around pH 2.8, whereas PZC of bare Fe_3O_4 nanoparticles is 6.7.[32] It has been found that AMNCs have a positive surface charge below their PZC, whereas negative surface charge above PZC. This difference in their charge characteristics may be attributed to the degree of ionization of functional groups at different pH values. On the other hand, the highly negative values of zeta potential of these nanoparticles in water (−26.6 mV) and 0.1 M phosphate buffered saline (PBS) (−26.0 mV) mediums also provide additional colloidal dispersibility to these particles. Further, dynamic light scattering (DLS, inset of Figure 2a) plot showed that these particles form a stable aqueous colloidal dispersion and have a mean number weighted hydrodynamic diameter of ~40 nm. This is significantly larger than the core size obtained by XRD and TEM. The observed higher hydrodynamic diameter is possibly due to the presence of an associated and hydrated AA layer on the surface of the particles. Further, the insignificant change in absorbance of particle suspension (0.1 mg/mL) in aqueous (water) and cell culture medium [Dulbecco's modified eagle medium (DMEM) with fetal bovine serum] with time (even after 72 h) indicates their good colloidal stability (Figure S2, Supporting Information). Thus, it can be predicted that the free hydroxyl groups of AA extend into the water medium, providing a high degree of aqueous colloidal stability to the particles. We also explored the interaction of AMNCs with bovine serum albumin (BSA) protein in a physiological medium (0.01 M PBS, pH 7.3). AMNCs do not show any significant change in zeta potential (Table S1, Supporting Information) even after interacting with BSA for 2 h, revealing their protein resistance characteristic in a physiological medium. This suggests that the suspension of these nanocarriers is suitable for applications under physiological conditions, which is essential for biomedical applications.

DOI: 10.1021/acsomega.9b01062
ACS Omega 2019, 4, 11728−11736

AMNCs exhibit superparamagnetic behavior without magnetic hysteresis and remanence (Figure 2b) at room temperature (RT). The maximum magnetization of AMNCs was found to be 56 emu/g at 20 kOe, which is equivalent to 60.8% of the bulk Fe_3O_4 (92 emu/g).[33] This decrease in magnetization can be attributed to both nano-sized Fe_3O_4 particles and random coating of AA on their surface.[34] However, the observed magnetization is comparable to that of bare Fe_3O_4 nanoparticles (60.5 emu/g) obtained by the co-precipitation method, reported earlier.[35] A similar value of maximum magnetization (67.6 emu/g) was obtained for bare Fe_3O_4 nanoparticles, prepared under similar conditions, without any passivating agent.[29] This further supports the coating of organic molecules as revealed by TGA and Fe estimation. In the presence of an external magnetic field (field strength of the magnet used is ~2.5 kOe), the opaque homogeneous dispersion of AMNCs changed to a clear and transparent solution within a few minutes (inset of Figure 2b). Thus, these water-dispersible Fe_3O_4 nanoparticles having a high magnetic response could be explored for various biomedical applications.

2.2. Drug Loading and Release Studies. The capability of AMNCs as a drug carrier was investigated by covalently conjugating the anticancer drug, DOX, through carbamate and hydrazone linkages. The interaction of DOX molecules with AMNCs was evident from the decrease in fluorescence intensity of the supernatant liquid obtained after removal of the drug-loaded AMNCs through magnetic separation (Figure 3a). The drug loading efficiencies of 48 and 57% were obtained for AMNCs-CL-DOX and AMNCs-HL-DOX, respectively, at DOX to particles' ratio of 1:10. A slightly higher loading efficiency was observed for hydrazone linkage than carbamate linkage. As evident from Scheme S1 (Supporting Information), the conjugation of DOX through carbamate linkage occurs through direct reaction between 4-nitrophenyl chloroformate (NPC)-activated AMNCs and amine group of DOX, whereas for hydrazone linkage it proceeds through a two-step reaction. In the first step, the NPC-activated AMNCs react with hydrazine, forming a nucleophilic substitution product. The easy accessibility of a less bulky nucleophile in a two-step reaction as opposed to a single-step process could significantly improve the yield of the reaction. This could be the probable reason for higher loading of DOX observed during hydrazone linkage. These pH-sensitive linkages (hydrazone and carbamate) can be cleaved at mild acidic pH, and thus provide opportunities for designing pH-responsive nanocarriers. The hydrodynamic diameter and surface charges of drug-loaded AMNCs were also investigated as these parameters are important criteria for drug delivery and provided in Table 1

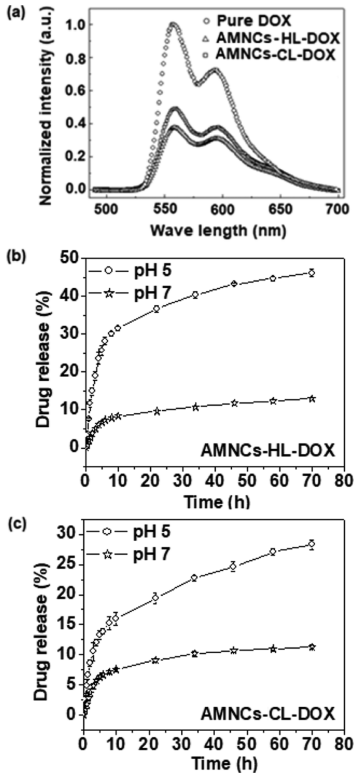

Figure 3. Fluorescence spectra showing interaction of DOX with AMNCs (a), pH-dependent drug release profile of AMNCs-HL-DOX (b), and AMNCs-CL-DOX (c) at 37 °C.

Table 1. Hydrodynamic Diameter (Number-Weighted) and Surface Charges of AMNCs, AMNCs-CL-DOX, and AMNCs-HL-DOX

MNPs system	zeta potential (mV)	hydrodynamic diameter (nm)	polydispersity index
AMNCs	−26.6	40	0.2
AMNCs-HL-DOX	−6.6	54	0.3
AMNCs-CL-DOX	−12.4	48	0.3

along with those of AMNCs. Further, TEM images of drug-loaded AMNCs confirmed the insignificant change in morphology of AMNCs after conjugation of DOX (Figure S3, Supporting Information).

The pH-dependent drug release profile of DOX-loaded AMNCs systems was investigated under different reservoir-sink conditions (reservoir: pH 5/pH 7.4 and sink: pH 7.4) at a temperature of 37 °C (Figure 3b,c). The physiological pH of the blood stream is 7.4, whereas sub-cellular lysosomal compartments of tumor cells have pH less than 5.0. The drug release studies (Figure 3b) show a strong dependence of the release profile on the reservoir pH values. Under these conditions, drug molecules release slowly over a period of 70 h with initial rapid release, followed by a slow, steady, and controlled release of the drug. The percentages of drug release from different drug-loaded systems are shown in Table 2.

Table 2. Percentage of Drug Release at Different Reservoir pHs in Buffer and Serum Mediums

	buffer mediums after 70 h		serum mediums after 10 h	
drug-loaded systems	pH 5	pH 7.4	pH 5	pH 7.4
AMNCs-HL-DOX	45	13	26	12
AMNCs-CL-DOX	28	11	16	11

Similar to our results, Aydin et al. reported much slower release of DOX from the cryogel system prepared through a relatively stable covalent bonding.[35] This is mainly due to the formation of stable linkage between drugs and nanocarriers. Between the two systems, the release rate of DOX from AMNCs-HL-DOX is slightly higher compared to AMNCs-CL-DOX because of the higher stability of carbamate linkage.[36] Further, it is noteworthy to mention that the release rate of DOX is higher at low pH for both the cases as carbamate and hydrazone linkages are prone to faster hydrolysis in acidic condition.

DOI: 10.1021/acsomega.9b01062
ACS Omega 2019, 4, 11728−11736

Thus, the release of DOX from the nanocarriers would increase in the acidic environment of the endosomal intracellular compartments after their internalization. The observed drug release characteristic is desirable for cancer therapy as DOX will be released at the targeted site. For instance, Prabaharan et al. reported that a covalently conjugated DOX-amphiphilic multiarm-block copolymer reduces the chance of premature drug release outside of the tumor tissue and shows excellent in vivo stability for targeting the drugs at cancer cells.[37] A significant difference in these covalently linked systems is that the percentage of drug release is much lower than that observed from noncovalently linked systems.[8,11] Further, the potential of the developed nanocarrier for delivery of DOX was evident from our short-term drug release study (Figure S4, Supporting Information) in serum mediums (Table 2). It showed pH-dependent release of DOX similar to that observed in buffer mediums (higher in acidic pH). The long-term (>10 h) release study could not be performed as fungal growth/protein aggregation was observed in release mediums beyond 10 h because of the presence of 10% fetal calf serum (FCS) in the release medium incubated at 37 °C.

2.3. Cytotoxicity and Cell Uptake Studies. The cytotoxicity of DOX-loaded AMNCs were investigated in cancer cells (WEHI-164, MCF-7, A549) as well as in normal cells (WI26VA4) (Figure 4). Our results showed an increase in cytotoxicity (30−60%) in these cancer cells when the cells were treated with increasing concentrations of AMNCs-CL-DOX/AMNCs-HL-DOX. However, the increase in cytotoxicity was not in a perfect dose-dependent manner. This could be attributed to the slow release of covalently bound DOX molecules from nanocarriers as cleavage of both carbamate and hydrazone linkages is quite a slow process. The toxicity observed was in a similar range across the three cancer cell lines used for both the drug-loaded AMNCs systems. However, DOX-loaded AMNCs showed relatively lower cytotoxicity as compared to pure DOX. This could be ascribed to the slower release of DOX from nanocarriers. It is noteworthy to mention that AMNCs-CL-DOX/AMNCs-HL-DOX showed significantly lower cytotoxicity (up to 20%) in human normal lung cells (WI26VA4), suggesting its relatively selective toxicity to cancer cells than normal cells. Moreover, the toxicity of AMNCs without conjugation of DOX observed in WI26VA4 was further lower (up to 20%), suggesting their biocompatibility (Figure S5, Supporting Information). The higher toxicity of AMNCs-CL-DOX/AMNCs-HL-DOX in normal cells than in AMNCs without conjugation of DOX may be attributed to the presence of DOX, which may impose higher inherent toxicity in normal cells.

Further, we have investigated the cellular uptake of DOX-loaded AMNC systems in WEHI-164 cells and compared it with that of pure DOX. In order to explore subcellular localization of DOX, the nuclei of the cells were stained with DAPI. The blue fluorescence image shows emission from DAPI-stained nuclei. As shown in Figure 5, WEHI-164 cells exposed to free DOX (magenta color arises from merged image of DOX and DAPI) showed nuclear internalization after 3 h, consistent with the earlier studies.[38,39] The accumulation of DOX in the nucleus for free DOX occurred as intracellular DOX molecules in the cytosol were observed to rapidly diffuse to the nucleus. In the case of DOX-loaded AMNCs, the red fluorescence signal coming up from DOX emissions was observed mainly in the cytoplasm. Thus, these nanocarriers have strong capability for intracellular delivery of anticancer drugs.

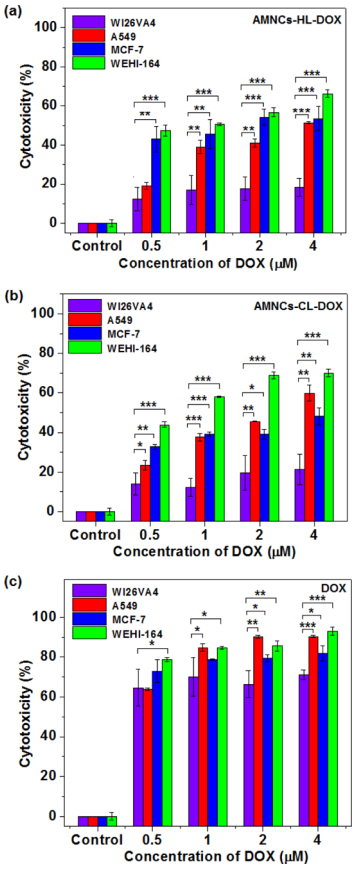

Figure 4. Cytotoxicity results of (a) AMNCs-HL-DOX, (b) AMNCs-CL-DOX, and (c) pure DOX toward cancer cells (WEHI-164, MCF-7, A549) and normal cells (WI26VA4) after 48 h of incubation at culture conditions. (Data represent the mean ± SD (n = 3); the statistically significant values were obtained using a t-test by comparing the toxicity of cancer cells with respect to normal cells, $^{*}p < 0.1$, $^{**}p < 0.01$, $^{***}p < 0.001$).

3. CONCLUSIONS

In summary, AA-functionalized Fe_3O_4 magnetic nanocarriers (~10 nm) were developed for slow and sustained delivery of covalently bound anticancer drug DOX to the tumor cells. These nanocarriers exhibit high water dispersibility, good magnetic field responsivity, biocompatibility, higher toxicity to tumor cells (than normal cells), protein resistance, and pH-dependent charge conversal features. It has been found that the loading efficiency of drugs as well as their pH-triggered release is strongly dependent on the nature of the bonding. The DOX−nanocarrier conjugates were found to be highly sensitive to acidic pH and reasonably stable at physiological pH. The higher release of DOX at mild acidic pHs such as those encountered in cancer cells may be due to the faster hydrolysis of carbamate and hydrazone linkage. These nanocarriers exhibit good cellular internalization and result in substantial cytotoxicity of DOX. The free hydroxyl group present on the surface of nanocarriers can provide accessible surfaces for conjugation of various biomolecules/biolabeling for a variety of other biomedical applications. Taken together, our results suggest the ability of these nanoparticles for pH-

DOI: 10.1021/acsomega.9b01062
ACS Omega 2019, 4, 11728−11736

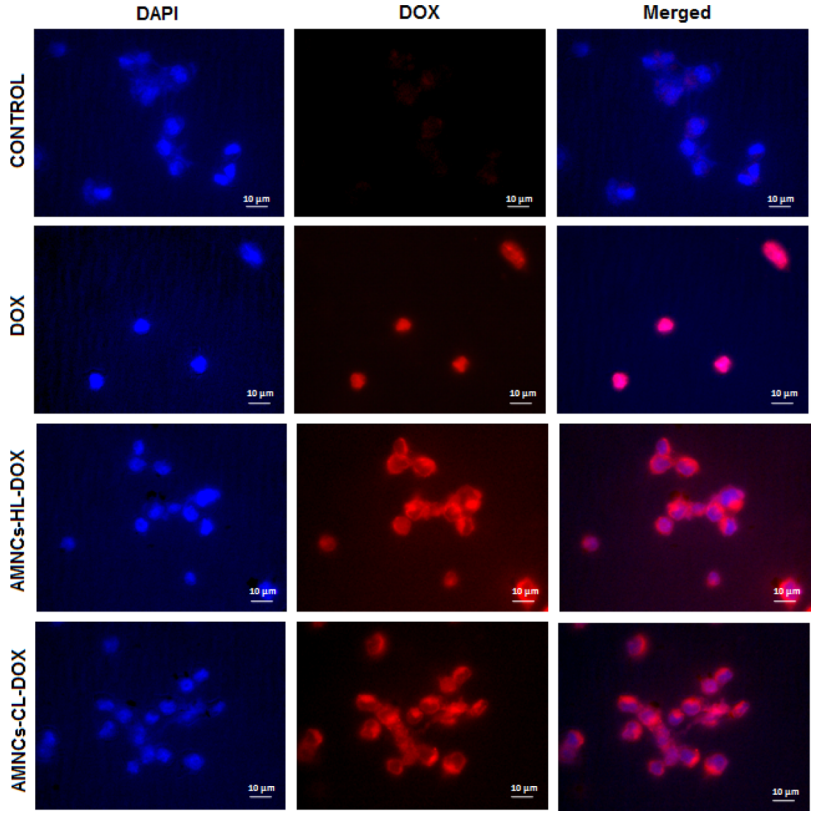

Figure 5. Fluorescence microscopy images of WEHI-164 cells after incubation with pure DOX and DOX-loaded AMNCs for 3 h under culture conditions (red filter for DOX and blue filter for DAPI, control cell with DAPI staining is provided for comparative purposes).

sensitive release of DOX and selective cytotoxicity to tumor cells.

4. EXPERIMENTAL SECTION

4.1. Materials. Ferrous chloride tetrahydrate ($FeCl_2{\cdot}4H_2O$, ≥99%), ferric chloride hexahydrate ($FeCl_3{\cdot}6H_2O$, ACS reagent, 97%), DOX (98%), BSA, and NPC were purchased from Sigma-Aldrich, USA. AA, ferrous ammonium sulphate, 1,10-phenanthroline monohydrate, hydrazine monohydrate, and dimethylformamide (DMF) were procured from Sisco Research Laboratories Pvt. Ltd., India. Triethylamine (TEA, ACS reagent, 99.5%) and dichloromethane (DCM) were bought from S. D. Fine Chem. Ltd., India. Ammonia solution (25%) was obtained from Thomas Baker Chemical Pvt. Ltd., India. Dialysis membrane-60 was procured from Himedia Laboratories Pvt. Ltd., India. The acetate buffer (AB, pH 5) and PBS (pH 7.4) were prepared using standard protocols. All chemicals used were of AR grade unless otherwise specified.

4.2. Synthesis of AA-Functionalized Fe_3O_4 Magnetic Particles (AMNCs). AMNCs were prepared by the co-precipitation method using a stoichiometric mixture of ferrous and ferric salts in aqueous medium followed by in situ coating of AA. Briefly, 0.994 g of $FeCl_2{\cdot}4H_2O$ and 2.703 g of $FeCl_3{\cdot}6H_2O$ (molar ratio of Fe^{2+}/Fe^{3+} = 1:2) were dissolved in 40 mL of oxygen-free Milli Q water in a round-bottom flask and the temperature was slowly increased to 80 °C in under nitrogen atmosphere with constant stirring. The temperature was maintained at 80 °C for 30 min and then 15 mL of 25% ammonia solution was added instantaneously to the reaction mixture, and kept for another 30 min at 70 °C. Then, 5 mL aqueous solution of AA (0.88 g) was added to the above reaction mixture. The temperature was slowly raised up to 90 °C and reacted for 60 min with continuous stirring for functionalization of particles with AA. The obtained black colored precipitates were then thoroughly rinsed 3−4 times with Milli Q water and separated from the supernatant using a permanent magnet of field strength ∼2.5 kOe.

4.3. Structural Characterizations and Magnetic Properties. An XRD study was done on a Rigaku diffractometer with Cu Kα radiation (λ = 1.540 nm). The crystallite size of AMNCs is estimated from the X-ray line broadening using Scherrer formula

$$\text{Crystallite size } (D) = \frac{0.89\,\lambda}{\beta \cos\theta}$$

where λ is the X-ray wavelength used, β is the angular line width at half-maximum intensity, and θ is Bragg's angle. Samples for TEM were prepared by sonicating particles in a liquid medium for 15 min and spreading a few drops on carbon-coated copper grids. After drying and keeping under vacuum for 2 h, the samples were examined under an FEI Tecnai T-20 having LaB6 filament located at the Tata Institute of Fundamental Research (TIFR), India. TEM micrographs were digitally recorded on a CCD camera and particle size was determined after examining at least 10 micrographs. The infrared spectra were recorded in the range of 4000−400 cm^{-1} on an FTIR spectrometer (Bomen Hartmann and Braun, MB series). TGA of the samples was carried out in the range of 40−500 °C at a scan rate of 10 °C/min under N_2 atmosphere. DLS measurement was performed using a Malvern 4800 Autosizer employing a 7132 digital correlator for the determination of hydrodynamic diameter. The zeta potential

DOI: 10.1021/acsomega.9b01062
ACS Omega 2019, 4, 11728−11736

measurements were determined by Zetasizer nanoseries, Malvern Instruments. The colloidal stability assay was investigated by measuring the absorbance of AMNCs suspensions (0.1 mg/mL) in different mediums (water and DMEM) at a wavelength of 350 nm using a JASCO V-650, UV−visible spectrophotometer. The magnetic measurements of AMNCs were carried out using a vibrating sample magnetometer (VSM, LakeShore, model-7410).

4.4. Drug Loading Studies. The anticancer drug DOX was used as a model drug to estimate the drug loading and release behavior of AMNCs. The covalent conjugation of DOX with AMNCs was carried out through carbamate and hydrazone linkage (Scheme 1) using the modified protocol reported by Hu et al. for preparation of biodegradable block copolymer−doxorubicin conjugates.[28] The detailed reaction pathway is shown in Scheme S1 (Supporting Information). For brevity, the DOX conjugated with AMNCs through carbamate linkage and hydrazone linkage are named as AMNCs-CL-DOX and AMNCs-HL-DOX, respectively.

AMNCs were first activated with NPC. Briefly, AMNCs (600 mg) were dissolved in 20 mL of DCM (CH_2Cl_2). Then, 100 mg of NPC and 200 μL of TEA were added drop wise to the above solution at 0 °C (molar ratio of AMNCs/NPC/TEA is 1:1.2:4). The reaction mixture was stirred at 0 °C for 4 h, and finally, the NPC-activated AMNCs were obtained through magnetic separation and washed 3−4 times with DCM to remove unreacted regents.

4.4.1. Covalent Conjugation via Carbamate Linkage (AMNCs-CL-DOX). The NPC-activated AMNCs (20 mg) dissolved in DMF (5 mL) was reacted with DOX (2 mg) in the presence of TEA (10 μL) for 48 h at RT under nitrogen atmosphere. The obtained product (AMNCs-CL-DOX) was then separated and washed 3−4 times with DMF through magnetic separation.

4.4.2. Covalent Conjugation via Hydrazone Linkage (AMNCs-HL-DOX). The NPC-activated AMNCs (50 mg) were dissolved in DCM (3 mL) and hydrazine monohydrate ($NH_2NH_2{\cdot}H_2O$) (22 μL) was slowly added into it. The reaction was carried out for 2 h at RT and hydrazine-modified AMNCs was separated and washed 3−4 times through magnetic separation. The hydrazine-modified AMNCs (20 mg) dissolved in DMF (5 mL) were reacted with DOX (2 mg) in the presence of TEA (50 μL) for 48 h at RT. The DOX-conjugated AMNCs (AMNCs-HL-DOX) were separated using a magnet and washed for 3−4 times by DMF.

4.4.3. Determination of Loading Efficiency. The fluorescence spectra of the supernatant (obtained after magnetic separation of DOX-loaded AMNCs) and pure DOX was recorded using a Hitachi F 4500 fluorescence spectrophotometer (λ_{ex}: 490 nm), (λ_{em}: 594 nm). The fluorescence intensities of the supernatants (washed drug molecules were also taken into consideration for calculations) against that of the pure DOX solution (prepared with appropriate mediums to maintain a similar condition) were used to determine the loading efficiency. The loading efficiency (w/w %) was calculated using the following relation

$$\text{Loading efficiency (\%)} = \frac{I_{DOX} - I_S - I_w}{I_{DOX}} \times 100$$

where I_{DOX} is the fluorescence intensity of the pure DOX solution, I_S the fluorescence intensity of the supernatant, and I_W the fluorescence intensity of the washed DOX (physically adsorbed DOX molecules).

4.5. Drug Release Studies. The pH-triggered drug release studies were carried out under reservoir (r)—sink (s) conditions. Drug-loaded particles were immersed into 5 mL of respective release mediums (AB—pH 5 or PBS 7.4) and then put into a dialysis bag. The dialysis was performed against 200 mL of PBS (pH 7.4) under continuous stirring at 37 °C to mimic the cellular environment. From the external medium, 1 mL was withdrawn at a fixed interval of time and replaced with fresh PBS to maintain the sink conditions. The amount of DOX released was determined by measuring the fluorescence intensity at 594 nm (λ_{ex}: 490 nm) using a microplate reader (Gen1.0.5, SYNERGY/H1 microplate reader; BioTeK, Germany) against the standard plot prepared under similar conditions. Each experiment was performed in triplicate and standard deviation was given in the plots. Further, drug release experiments were also performed in serum conditions (prepared by adding 10% FCS to the respective buffer medium) under similar conditions as mentioned above.

4.6. Cytotoxicity and Cell Uptake Studies. An MTT assay was used to investigate the cytotoxicity of AMNCs, DOX-loaded AMNCs (AMNCs-CL-DOX, AMNCs-HL-DOX), and pure DOX against three different cancer cell lines, WEHI-164 (mouse fibrosarcoma cells), MCF-7 (human breast cancer cells), and A549 (human lung cancer cells), and one normal cell line, WI26VA (human normal lung cells). The cancer and normal cell lines were obtained from the National Centre for Cell Sciences, Pune, India, and Sigma-Aldrich, USA, respectively. The cells were cultured in DMEM supplemented with 10% FCS and antibiotics (100 U mL^{-1} penicillin and 100 μg mL^{-1} streptomycin) cultured in a humidified atmosphere of 5% CO_2 at 37 °C. The cells (5000) were seeded in 96-well plates containing 100 μL of culture medium overnight in culture conditions. For determining the cytotoxicity, the cells were treated with different concentrations of drug-loaded AMNCs/controls followed by incubation at culture conditions for 48 h. After this, the culture medium of each well was replaced by a fresh medium containing 0.5 mg/mL MTT and further incubated for 3 h at culture conditions. Following this, the MTT solution was aspirated, and formazan crystals were solubilized by adding 100 μL of dimethyl sulfoxide (DMSO) to each well. For determining the cytotoxicity, the absorbance was measured in a microplate reader (Tecan Infinite 200 PRO, Switzerland) at 544 nm. The cell toxicity was obtained by comparing the absorption of the treated cells to that of the control, which was defined as 100%. Each experiment was performed in triplicate and the standard deviation was given in the plot.

Cellular uptake of drug-loaded AMNCs was investigated using WEHI-164 cells by fluorescence microscopy. For fluorescence imaging, cells (0.5×10^6) were seeded on glass coverslips and cultured overnight. The cells were then treated with AMNCs-CL-DOX/AMNCs-HL-DOX (at a DOX concentration of 4 μM) and incubated for 3 h under culture conditions, followed by washing with PBS. The untreated control cells and the cells treated with drug-loaded AMNCs were mounted on a glass slide in a cell mounting medium (Invitrogen, USA) containing DAPI for nuclear staining and then imaged by fluorescence microscopy (Nikon Eclipse Ti, Japan) using a red filter for DOX and a blue filter for DAPI.

DOI: 10.1021/acsomega.9b01062
ACS Omega 2019, 4, 11728−11736

■ ASSOCIATED CONTENT

Supporting Information

The Supporting Information is available free of charge on the ACS Publications website at DOI: 10.1021/acsomega.9b01062.

Particle size distribution, selected area electron diffraction pattern, normalized absorbance versus time plot, TEM micrographs, drug release profile, cytotoxicity, zeta potential results, and detailed reaction pathway (PDF)

■ AUTHOR INFORMATION

Corresponding Authors

*E-mail: kcbarick@barc.gov.in (K.C.B.).
*E-mail: hassan@barc.gov.in (P.A.H.).

ORCID

Puthussericka A. Hassan: 0000-0001-7137-4788

Notes

The authors declare no competing financial interest.

■ ACKNOWLEDGMENTS

The authors acknowledge Prof. D. Bahadur, Indian Institute of Technology, Bombay, India, for his encouragement and facilitating the use of VSM.

■ REFERENCES

(1) Tannock, I. F. Conventional cancer therapy: promise broken or promise delayed? *Lancet* **1998**, *351*, SII9−SII16.

(2) Shi, J.; Kantoff, P. W.; Wooster, R.; Farokhzad, O. C. Cancer nanomedicine: progress, challenges and opportunities. *Nat. Rev. Cancer* **2017**, *17*, 20−37.

(3) Wei, K.-C.; Yang, H.-W.; Hua; Liu; Huang. Potential of magnetic nanoparticles for targeted drug delivery. *Nanotechnol Sci Appl* **2012**, *5*, 73−86.

(4) Sahoo, B.; Devi, K. S. P.; Banerjee, R.; Maiti, T. K.; Pramanik, P.; Dhara, D. Thermal and pH responsive polymer-tethered multifunctional magnetic nanoparticles for targeted delivery of anticancer drug. *ACS Appl. Mater. Interfaces* **2013**, *5*, 3884−3893.

(5) Chandra, S.; Dietrich, S.; Lang, H.; Bahadur, D. Dendrimer-doxorubicin conjugate for enhanced therapeutic effects for cancer. *J. Mater. Chem.* **2011**, *21*, 5729−5737.

(6) Gupta, A. K.; Gupta, M. Synthesis and surface engineering of iron oxide nanoparticles for biomedical applications. *Biomaterials* **2005**, *26*, 3995−4021.

(7) Barick, K. C.; Aslam, M.; Lin, Y.-P.; Bahadur, D.; Prasad, P. V.; Dravid, V. P. Novel and efficient MR active aqueous colloidal Fe_3O_4 nanoassemblies. *J. Mater. Chem.* **2009**, *19*, 7023−7029.

(8) Barick, K. C.; Singh, S.; Jadhav, N. V.; Bahadur, D.; Pandey, B. N.; Hassan, P. A. pH-Responsive Peptide Mimic Shell Cross-Linked Magnetic Nanocarriers for Combination Therapy. *Adv. Funct. Mater.* **2012**, *22*, 4975−4984.

(9) Laurent, S.; Forge, D.; Port, M.; Roch, A.; Robic, C.; Vander Elst, L.; Muller, R. N. Magnetic iron oxide nanoparticles: Synthesis, stabilization, vectorization, physicochemical characterizations, and biological applications. *Chem. Rev.* **2008**, *108*, 2064−2110.

(10) Chandra, S.; Barick, K. C.; Bahadur, D. Oxide and hybrid nanostructures for therapeutic applications. *Adv. Drug Delivery Rev.* **2011**, *63*, 1267−1281.

(11) Nigam, S.; Barick, K. C.; Bahadur, D. Development of citrate-stabilized Fe_3O_4 nanoparticles: Conjugation and release of doxorubicin for therapeutic applications. *J. Magn. Magn. Mater.* **2011**, *323*, 237−243.

(12) Dutta, B.; Shetake, N. G.; Barick, B. K.; Barick, K. C.; Pandey, B. N.; Priyadarsini, K. I.; Hassan, P. A. pH sensitive surfactant-stabilized Fe3O4 magnetic nanocarriers for dual drug delivery. *Colloids Surf., B* **2018**, *162*, 163−171.

(13) Sreeja, V.; Jayaprabha, K. N.; Joy, P. A. Water-dispersible ascorbic-acid-coated magnetite nanoparticles for contrast enhancement in MRI. *Appl. Nanosci.* **2015**, *5*, 435−441.

(14) Gupta, H.; Paul, P.; Kumar, N.; Baxi, S.; Das, D. P. One pot synthesis of water-dispersible dehydroascorbic acid coated Fe_3O_4 nanoparticles under atmospheric air: blood cell compatibility and enhanced magnetic resonance imaging. *J. Colloid Interface Sci.* **2014**, *430*, 221−228.

(15) Xiao, L.; Li, J.; Brougham, D. F.; Fox, E. K.; Feliu, N.; Bushmelev, A.; Schmidt, A.; Mertens, N.; Kiessling, F.; Valldor, M.; Fadeel, B.; Mathur, S. Water-soluble superparamagnetic magnetite nanoparticles with biocompatible coating for enhanced magnetic resonance imaging. *ACS Nano* **2011**, *5*, 6315−6324.

(16) Rajh, T.; Nedeljkovic, J. M.; Chen, L. X.; Poluektov, O.; Thurnauer, M. C. Surface modification of small particle TiO_2 colloids with cysteine for enhanced photochemical reduction:An EPR Study. *J. Phys. Chem. B* **1999**, *103*, 3515−3519.

(17) Mowry, S.; Ogren, P. J. Kinetics of methylene blue reduction by ascorbic acid. *J. Chem. Educ.* **1999**, *76*, 970.

(18) Rivas, C. I.; Zúñiga, F. A.; Salas-Burgos, A.; Mardones, L.; Ormazabal, V.; Vera, J. C. Vitamin C transporters. *J. Physiol. Biochem.* **2008**, *64*, 357−375.

(19) Macheda, M. L.; Rogers, S.; Best, J. D. Molecular and cellular regulation of glucose transporter (GLUT) proteins in cancer. *J. Cell. Physiol.* **2005**, *202*, 654−662.

(20) Agus, D. B.; Gambhir, S. S.; Pardridge, W. M.; Spielholz, C.; Baselga, J.; Vera, J. C.; Golde, D. W. Vitamin C crosses the blood-brain barrier in the oxidized form through the glucose transporters. *J. Clin. Invest.* **1997**, *100*, 2842−2848.

(21) Liang, J.-J.; Zhou, Y.-Y.; Wu, J.; Ding, Y. Gold Nanoparticle-based drug delivery platform for antineoplastic chemotherapy. *Curr. Drug Metab.* **2014**, *15*, 620−631.

(22) Zhu, Y.-J.; Chen, F. pH-responsive drug-delivery systems. *Chem.—Asian J.* **2015**, *10*, 284−305.

(23) Sawant, R. M.; Hurley, J. P.; Salmaso, S.; Kale, A.; Tolcheva, E.; Levchenko, T. S.; Torchilin, V. P. "SMART" Drug Delivery Systems: Double-Targeted pH-Responsive Pharmaceutical Nanocarriers. *Bioconjugate Chem.* **2006**, *17*, 943−949.

(24) Aryal, S.; Hu, C.-M. J.; Zhang, L. Polymer−Cisplatin Conjugate Nanoparticles for Acid-Responsive Drug Delivery. *ACS Nano* **2010**, *4*, 251−258.

(25) Zhang, Y.; Yang, C.; Wang, W.; Liu, J.; Liu, Q.; Huang, F.; Chu, L.; Gao, H.; Li, C.; Kong, D.; Liu, Q.; Liu, J. Co-delivery of doxorubicin and curcumin by pH-sensitive prodrug nanoparticle for combination therapy of cancer. *Sci. Rep.* **2016**, *6*, 21225.

(26) Liu, Y.; Wang, W.; Yang, J.; Zhou, C.; Sun, J. pH-sensitive polymeric micelles triggered drug release for extracellular and intracellular drug targeting delivery. *Asian J. Pharm. Sci.* **2013**, *8*, 159−167.

(27) Rollas, S.; Kucukguzel, S. G. Hydrazone, amide, carbamate, macromolecular and other prodrugs of doxorubicin. *Open Drug Deliv. J.* **2008**, *2*, 77−85.

(28) Hu, X.; Liu, S.; Huang, Y.; Chen, X.; Jing, X. Biodegradable block copolymer-doxorubicin conjugates via different linkages: Preparation, characterization, and in vitro evaluation. *Biomacromolecules* **2010**, *11*, 2094−2102.

(29) Majeed, J.; Barick, K. C.; Shetake, N. G.; Pandey, B. N.; Hassan, P. A.; Tyagi, A. K. Water-dispersible polyphosphate grafted Fe_3O_4 nanomagnets for cancer therapy. *RSC Adv.* **2015**, *5*, 86754−86762.

(30) Juhász, M.; Kitahara, Y.; Takahashi, S.; Fujii, T. Thermal stability of vitamin C: Thermogravimetric analysis and use of total ion monitoring chromatograms. *J. Pharm. Biomed. Anal.* **2012**, *59*, 190−193.

(31) Ding, B.; Xia, S.; Hayat, K.; Zhang, X. Preparation and pH stability of ferrous glycinate liposomes. *J. Agric. Food Chem.* **2009**, *57*, 2938−2944.

(32) Chang, Y.-C.; Chen, D.-H. Preparation and adsorption properties of monodisperse chitosan-bound Fe_3O_4 magnetic nano-

DOI: 10.1021/acsomega.9b01062
ACS Omega 2019, 4, 11728−11736

particles for removal of Cu(II) ions. *J. Colloid Interface Sci.* **2005**, *283*, 446−451.
(33) Yamaura, M.; Camilo, R. L.; Sampaio, L. C.; Macêdo, M. A.; Nakamura, M.; Toma, H. E. Preparation and characterization of (3-aminopropyl)triethoxysilane-coated magnetite nanoparticles. *J. Magn. Magn. Mater.* **2004**, *279*, 210−217.
(34) Mikhaylova, M.; Kim, D. K.; Bobrysheva, N.; Osmolowsky, M.; Semenov, V.; Tsakalakos, T.; Muhammed, M. Superparamagnetism of magnetite nanoparticles: Dependence on surface modification. *Langmuir* **2004**, *20*, 2472−2477.
(35) Zhang, Y.-Q.; Wei, X.-W.; Yu, R. Fe_3O_4 nanoparticles-supported palladium-bipyridine complex: effective catalyst for Suzuki coupling reaction. *Catal. Lett.* **2010**, *135*, 256−262.
(36) Aydin, D.; Arslan, M.; Sanyal, A.; Sanyal, R. Hooked on cryogels: A carbamate linker based depot for slow drug release. *Bioconjugate Chem.* **2017**, *28*, 1443−1451.
(37) Prabaharan, M.; Grailer, J. J.; Pilla, S.; Steeber, D. A.; Gong, S. Amphiphilic multi-arm-block copolymer conjugated with doxorubicin via pH-sensitive hydrazone bond for tumor-targeted drug delivery. *Biomaterials* **2009**, *30*, 5757−5766.
(38) Gillies, E. R.; Fréchet, J. M. J. pH-responsive copolymer assemblies for controlled release of doxorubicin. *Bioconjugate Chem.* **2005**, *16*, 361−368.
(39) Zhao, H.; Yung, L. Y. L. Selectivity of folate conjugated polymer micelles against different tumor cells. *Int. J. Pharm.* **2008**, *349*, 256−268.

DOI: 10.1021/acsomega.9b01062
ACS Omega 2019, 4, 11728−11736